CRYSTAL GROWTH & DESIGN

pubs.acs.org/crystal

Article

Ritonavir Form III: A Coincidental Concurrent Discovery

Stephan D. Parent, Pamela A. Smith, Dale K. Purcell, Daniel T. Smith, Susan J. Bogdanowich-Knipp, Ami S. Bhavsar, Larry R. Chan, Jordan M. Croom, Haley C. Bauser, Andrew McCalip, Stephen R. Byrn, and Adrian Radocea*

Cite This: *Cryst. Growth Des.* 2023, 23, 320−325

Read Online

ACCESS | Metrics & More | Article Recommendations | Supporting Information

ABSTRACT: Polymorph screening is a crucial step in the characterization and development of pharmaceuticals. The 1998 recall of ritonavir upon the unexpected appearance of the more stable Form II polymorph remains a notorious case of disappearing polymorphs as the presence of Form II inhibited the ability to grow the original Form I. This study presents the characterization of Form III of ritonavir grown from melt/cool crystallization. While Form III was observed in 2014, it was not characterized as a unique polymorph until 2022 when, coincidentally, a team at AbbVie and the authors of this manuscript independently discovered Form III via melt/cool crystallization. This study builds upon the discovery through a thorough characterization and novel thermal profile for quicker nucleation and crystallization of the new form.

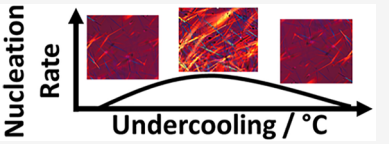

INTRODUCTION

Since the ritonavir crisis in 1998, when the lifesaving HIV protease inhibitor had to be withdrawn from the market for almost a year due to a sudden and unpredictable appearance of a new less-soluble polymorph, ritonavir has been of interest to solid state chemists, crystallographers, and drug development scientists.[1−4] The phenomenon of disappearing polymorphs is defined by cases in which the discovery of a new, frequently more stable polymorph renders the existing polymorph nearly impossible to produce.[2,5−9] In 2015, a review on disappearing polymorphs highlighted the appearance of ritonavir Form II as perhaps "the most notorious example of disappearing polymorphs."[2]

Thorough polymorph screening is crucial in the understanding of active pharmaceutical ingredients as different polymorphs may exhibit variations in solubility, bioavailability, stability, and other critical properties in the evaluation of a drug.[1,4,10,11] There are many techniques to induce crystallization for polymorph screening including antisolvent methods, solution-based methods, evaporation methods, high-pressure crystallization, and crystallization from the melt.[4,11−20] While many recent studies on ritonavir relate to its performance as an amorphous solid dispersion, there have been recent advances in understanding the crystallization of ritonavir.[4,21−25] After the appearance of Form II ritonavir, two new solvates and an anhydrous form were discovered by Morissette et al.[4] In 2014, Kawakami et al. published their findings after crystallizing ritonavir from its melt. They detected the appearance of a crystalline form after annealing in a 60 °C oven over a period of several days.[24] They concluded that the material was Form IV identified by Morissette et al.[4,24] However, the X-ray powder diffraction (XPRD) patterns labeled as such do not match the Form IV XRPD pattern in the publication by Morissette et al.[4,24]

In 2022 Yao et al. published a rapid communication, reporting a new anhydrous form, labeled as Form III ritonavir.[25] An overlay of the Form III pattern reported by Yao et al. and the "Form IV" pattern in a 2014 publication by Kawakami et al. suggest that the "Form IV" pattern in the paper was actually a mixture of the new Form III reported by Yao et al. and amorphous material.[24,25] It appears as if Kawakami et al. discovered Form III but did not recognize that it was a new form. To clarify, the label Form III was previously used by Morisette et al. to identify a crystalline solvate.[4] However, this communication follows the Form III naming convention adopted by Yao et al.[25]

Coincidentally, our team was investigating the crystallization of ritonavir from its melt concurrently with Yao et al., and also identified and characterized Form III. This paper reports that method and several previously unreported properties of Form III ritonavir, demonstrating the value of thermal methods in the discovery of ritonavir polymorphs.

METHODS

Microcrystallization (Samples 1a−1e). Form III was confirmed via Raman microscopy of several samples created during various hot-stage optical microscopy (HSOM) experiments. For each experiment, a small portion (∼0.5 mg) of ritonavir Form II was placed on a scrupulously clean microscope slide. The sample was not covered with a cover glass. The Linkam hot-stage system controller was

Received: September 9, 2022
Revised: December 5, 2022
Published: December 21, 2022

Table 1. Thermal Profiles of Ritonavir Microcrystallization

	sample 1a	sample 1b	sample 1c	sample 1d	sample 1e
step 1	heat 40 °C/min to 127.0 °C hold for 1 min	heat 40 °C/min to 127.0 °C hold for 1 min	heat 40 °C/min to 127.0 °C hold for 1 min	heat 40 °C/min to 127.0 °C hold for 1 min	heat 40 °C/min to 127.0 °C hold for 2 min
step 2	cool 20 °C/min to 70 °C hold for 20 h	cool 20 °C/min to 80 °C hold for 20 h	cool 20 °C/min to 80 °C hold for 20 h	cool 20 °C/min to 80 °C hold for 8 h	cool 20 °C/min to 30 °C hold for 1 h
step 3	cool 2 °C/min to 30 °C hold for 5 h	cool 2 °C/min to 30 °C hold for 4 h	cool 2 °C/min to 30 °C hold for 5 h	cool 2 °C/min to 30 °C hold for 5 h	heat 2 °C/min to 80 °C hold for 10 h
step 4	N/A	N/A	N/A	N/A	cool 2 °C/min to 30 °C hold for 10 h
Raman results	amorphous, Form III	Form II, Form III, unknown	Form III	amorphous, Form III	amorphous, Form III

programmed with various temperature ramp routines, as described in Table 1.

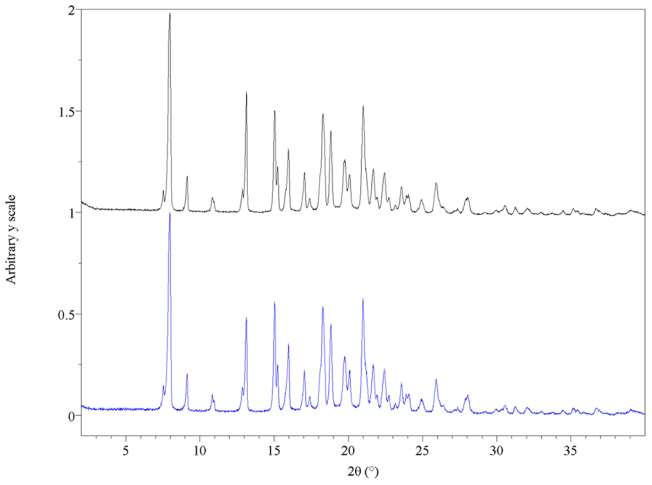

Figure 1. X-ray powder diffraction patterns for ritonavir Form III obtained at the macroscale, samples 1f (top, black) and 1g (bottom, blue).

In sample 1d, nucleation was evident within 7 min and 35 s of reaching 80 °C (during step 2), and in sample 1e, nucleation was evident within 17 min and 15 s of reaching 80 °C (during step 3). Directly upon completion of the hot-stage temperature ramp routine, a few crystals of the sample were transferred to either a gold-coated microscope slide or a fused-silica microscope slide and analyzed by Raman microscopy using a HORIBA Scientific XploRA Series Confocal Raman Microscope. A fused silica slide was used in sample measurements unaffected by the substrate's inherent Raman signal. A gold-coated microscope slide was used in the analysis of smaller samples.

Macrocrystallization (Samples 1f−1g). Samples 1f and 1g were prepared by starting with 150.0 mg of ritonavir USP lot M-RIT/0804007 Form II flattened on a glass slide to provide a solid compact of uniform thickness of approximately 1 mm × 17 mm × 17 mm (289 mm^3) in size. Using a drying oven, both samples were melted by exposure to 125−128 °C for 17 min. Temperatures near the vicinity of the sample were measured with a mercury thermometer placed directly next to or suspended directly above the sample within the oven. The complete melt was confirmed visually. Sample 1f was held at 128 °C for an additional 10 min to ensure that no crystalline particles of Form II remained within the melt. The melts were immediately transferred to a second drying oven and placed near a mercury thermometer, also within the oven, measuring 80 °C. Sample 1f was retained at the growth temperature for 37 h, and sample 1g was retained at the growth temperature for 23 h. The samples, undisturbed from the glass slide, were removed from the oven and observed with an Olympus SZX9 stereomicroscope under crossed polarizers as a dense mat of birefringent needles. Raman microscopy was performed using a HORIBA Scientific XploRA Series Confocal Raman Microscope. The material was removed from the glass slide and rendered into a powder and analyzed by XPRD, with a PANalytical Empyrean diffractometer and PIXcel3D-Medipix3 1 × 1 detector located 240 mm from the specimen and differential scanning calorimetry (DSC) using a TA Instruments model Q10. Details of the measurement methods are outlined in the Supporting Information.

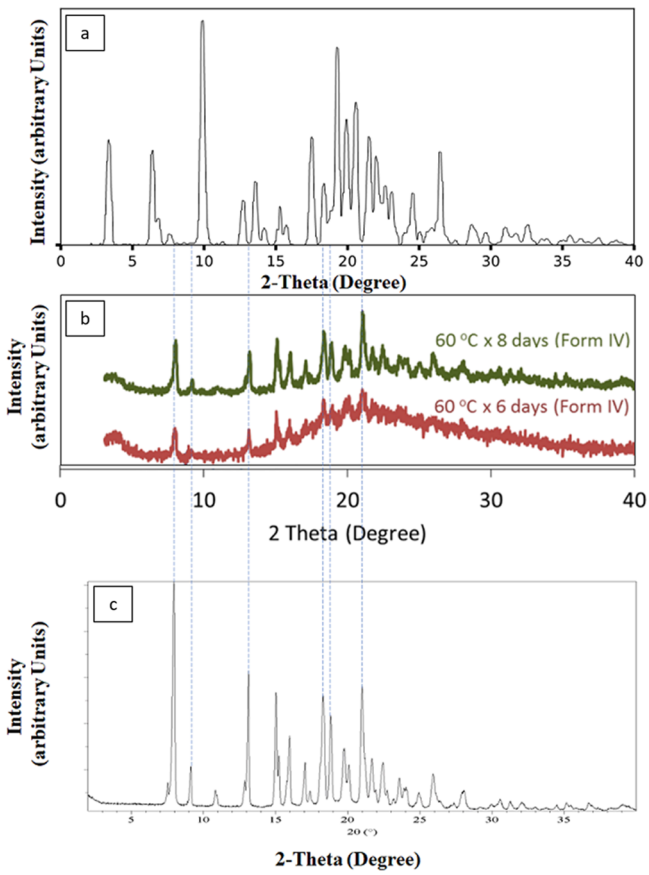

Figure 2. Comparison of XPRD patterns of (a) Morissette et al.'s Form IV, (b) Kawakami "Form IV", and (c) herein presented Form III.[4,24] (b) Adapted with permission.[24] Copyright 2014, American Chemical Society.

A 150.0 mg sample of ritonavir USP lot M-RIT/0804007 Form II was flattened on a glass slide to provide a solid compact of uniform thickness of approximately 1 mm × 17 mm × 17 mm (289 mm^3) in size. Using a drying oven, the compact was melted by exposure to 125−128 °C for 27 min. The melt was immediately transferred to a second drying oven and placed near a mercury thermometer, also within the oven, measuring 80 °C, and remained there for 23 h. The sample, undisturbed from the glass slide, was removed from the oven and observed with an Olympus SZX9 stereomicroscope under crossed polarizers as a dense mat of birefringent needles. The material was

https://doi.org/10.1021/acs.cgd.2c01017
Cryst. Growth Des. 2023, 23, 320−325

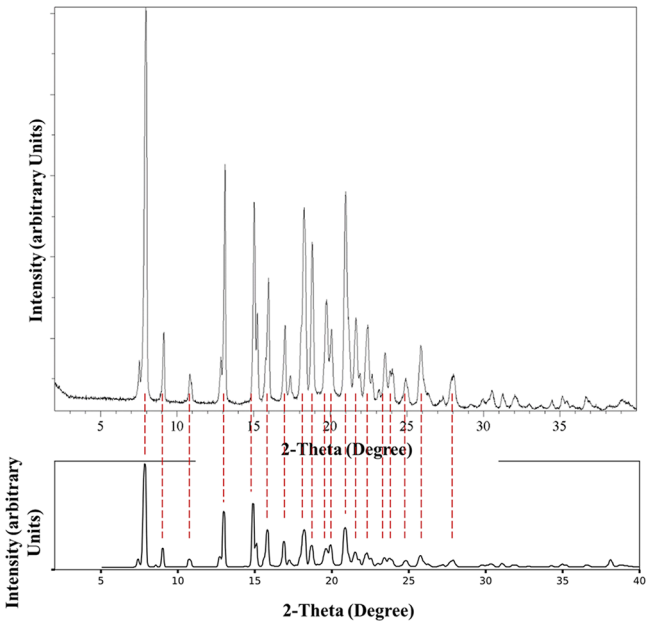

Figure 3. Comparison of XPRD patterns for Form III obtained herein and collected by Yao et al.[25]

removed from the glass slide and rendered into a powder and analyzed by XPRD. The assigned sample number for this material was 1g, and measurement specifications are detailed in the Supporting Information.

RESULTS AND DISCUSSION

Figure 1 shows the X-ray diffraction patterns of Form III isolated in samples 1f and 1g (top and bottom, respectively). Figure 2 shows a comparison of XPRD patterns across Morissette et al.'s Form IV, the Kawakami "Form IV" (green and red diffractograms), and Form III characterized in this work.[4,24] The three combined figures are presented with the *x* axes on the same scale, to facilitate comparison. Vertical dotted lines facilitate comparison of the diffraction peaks for Form III, clearly indicating that the Kawakama patterns do not match Morissette et al.'s Form IV and in fact match the new Form III.[4,24] Finally, the XRPD pattern of Form III identified in this work is compared to the XRPD pattern shown by Yao et al. for Form III in Figure 3.[25] Dotted lines are provided to aid comparison, confirming the match.

Table 2. Pawley Refinement Parameters

space group	C2	cell volume (Å^3)	4031.5
a (Å)	23.656	*α* (°)	90
b (Å)	5.031	*β* (°)	90.572
c (Å)	33.878	*γ* (°)	90

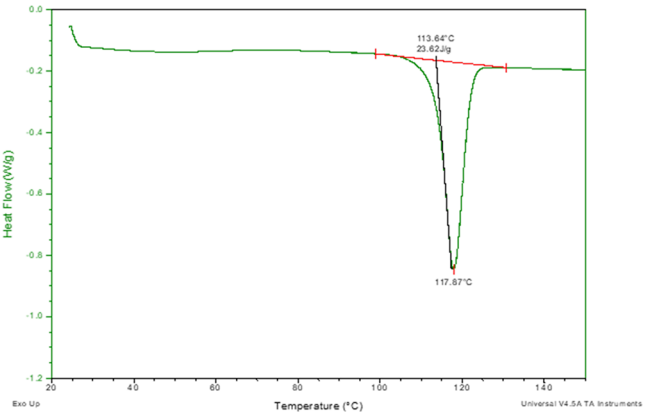

Figure 5. Differential scanning calorimetry thermogram for ritonavir Form III (sample 1f).

Table 3. Raman Microscopy Results on HSOM Experiments

sample	Raman results (number of spectra providing results, out of 10)
1a	amorphous (two spectra), Form III (three spectra), mixture amorphous and Form III (three spectra)
1b	Form II (four spectra), Form III (five spectra), unknown (one spectrum)
1c	Form III (10 spectra)
1d	amorphous (three spectra), Form III (one spectrum), mixture amorphous and Form III (six spectra)
1e	amorphous (one spectrum), Form III (five spectra), mixture amorphous and Form III (four spectra)

The X-ray pattern obtained on Form III sample 1f was analyzed using an indexing method.[26] Indexing is a computational method that searches for a set of crystallographic space group and unit cell parameters that best match the observed Bragg angles in a powder pattern. If successful and all observed Bragg peaks can be attributed to the indexing solution, it is highly likely the XRPD pattern represents a single crystalline phase. The indexing solution can then be used to perform

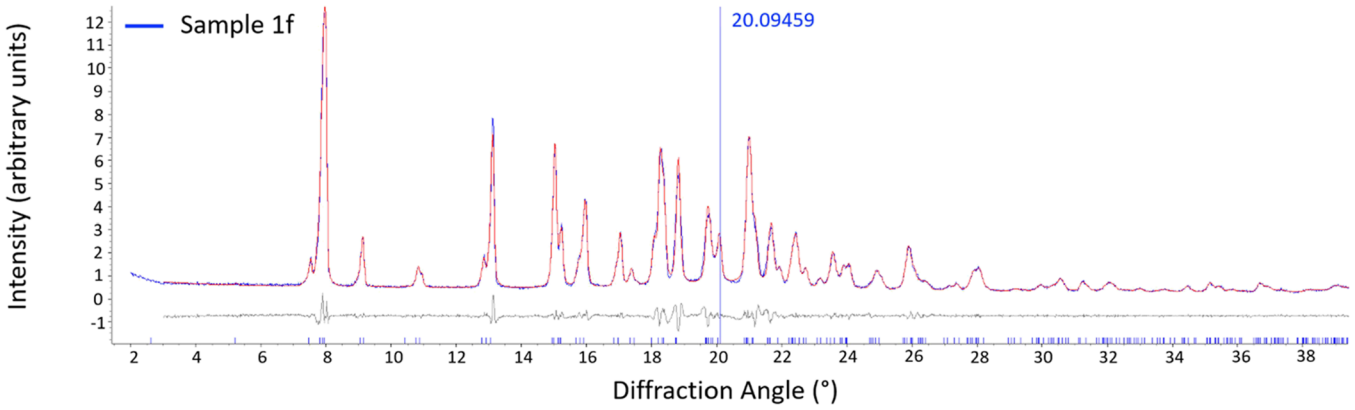

Figure 4. Indexing and Pawley refinement of Form III (sample 1f). Blue: experimental data; red: fit; gray: fit residual; and blue notches: allowed peak positions.

https://doi.org/10.1021/acs.cgd.2c01017
Cryst. Growth Des. 2023, 23, 320−325

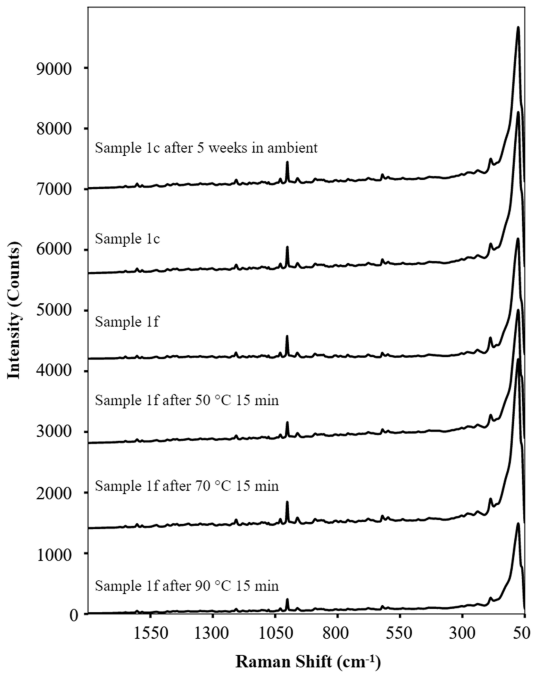

Figure 6. Raman spectra of Form III obtained from microcrystallization (sample 1c) and macrocrystallization (sample 1f) experiments. Spectra of sample 1f were collected before and after exposing the sample to 50, 70, and 90 °C for 15 min. Sample 1c was reexamined after 5 weeks in ambient conditions. Each spectrum is an average of 10 separate spectra collected for each sample, other than spectra for sample 1f after exposure to elevated temperatures, in which case each spectrum is an average of 5 spectra. Form III remains unchanged.

whole-pattern Pawley refinement to accurately determine the unit cell volume and cell parameters and investigate the fit residual for crystalline phase impurities.[27] The successful indexing solution from the pattern is shown in Figure 4, and the cell parameters are shown in Table 2. Additional details on the Pawley refinement are given in the Supporting Information. The unit cell parameters are identical, within the expected experimental error, to those published in Yao et al.[25] The differences are attributed to the temperatures at which the powder pattern (at ambient temperature) and the single crystal data (at 150 K) were acquired. Low temperatures are used in single crystal analysis to improve the quality of the structure but can contract the crystal resulting in a change in the unit cell parameters.

Form III was also characterized by three thermal techniques: DSC, HSOM, and thermogravimetric (TG) analysis. The DSC curve is displayed in Figure 5. TG analysis is shown in the Supporting Information. The sample has a melt onset temperature of ∼114 °C, with the endotherm maximum near 118 °C.

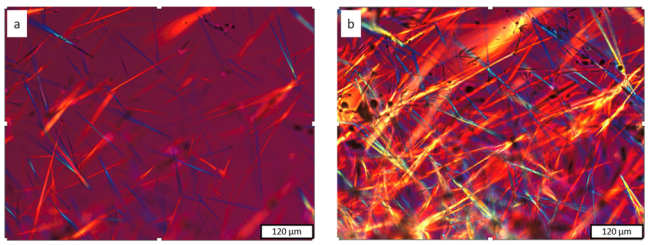

Figure 8. HSOM images of Form III crystals grown at 80 °C from the supercooled melt after (a) 5 h and (b) 8 h.

Results from the HSOM investigation for the melting point of Form III indicated an onset temperature of 113.7 °C, matching the DSC data. The sample was completely melted by 117.9 °C and did not recrystallize upon cooling to 26.2 °C. These results conform to the DSC results.

Several crystals that were created during the HSOM experiments (microcrystallizations) were subsequently analyzed by Raman microscopy. At least five spectra were collected for each sample. In some cases, more than one form was found in each sample. Table 3 summarizes the Raman findings.

Raman spectra were also obtained from the macrocrystallization sample (1f). Figure 6 displays the Form III spectrum from the macroexperiment along with a representative Form III spectrum from the microcrystallization experiments (sample 1c). The lattice modes in the low-frequency range are included specifically to show that Form III maintained its crystallinity and did not change across storage conditions. The spectra match each other, and they match the Raman spectra reported for Form III by Yao et al.[25]

Stability analyses were conducted on Form III (1f) by holding the material sequentially for 15 min at 50 °C, 15 min at 70 °C, and 15 min at 90 °C. The sample was analyzed by Raman microscopy after each temperature exposure. In all cases, the material remained as Form III. Lastly, sample 1c from Table 1 was re-analyzed after storage under ambient conditions for 5 weeks as an additional stability test. Form III (sample 1c) remained unchanged after 5 weeks.

The optimal nucleation and growth strategy for Form III ritonavir was determined qualitatively from HSOM microcrystallization experiments. The images shown in Figure 7 compare relative concentrations of crystals within the supercooled melt when incubated for 5 h at each of the indicated temperatures. Nucleation did not occur at 100 °C (not shown). The lowest concentration of crystals is evident at both 90 and 70 °C, indicating that nucleation and/or growth is (are) slow under either condition. The highest concentration of well-formed needles is observed when held at 80 °C. Given

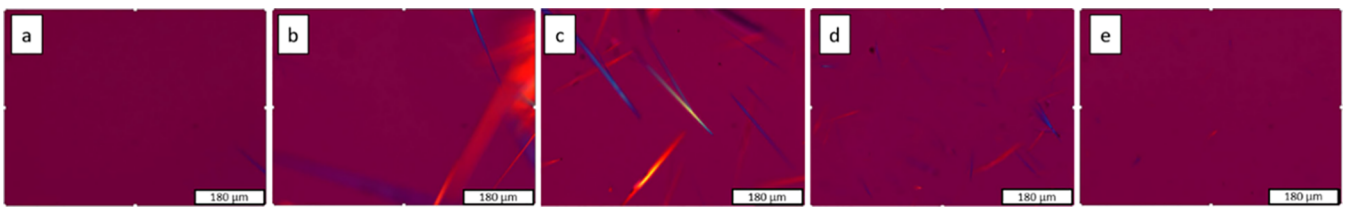

Figure 7. HSOM images of Form III crystals grown from supercooled melts when incubated for 5 h at: (a) 90 °C; (b) 85 °C; (c) 80 °C; (d) 75 °C; and (e) 70 °C.

https://doi.org/10.1021/acs.cgd.2c01017
Cryst. Growth Des. 2023, 23, 320−325

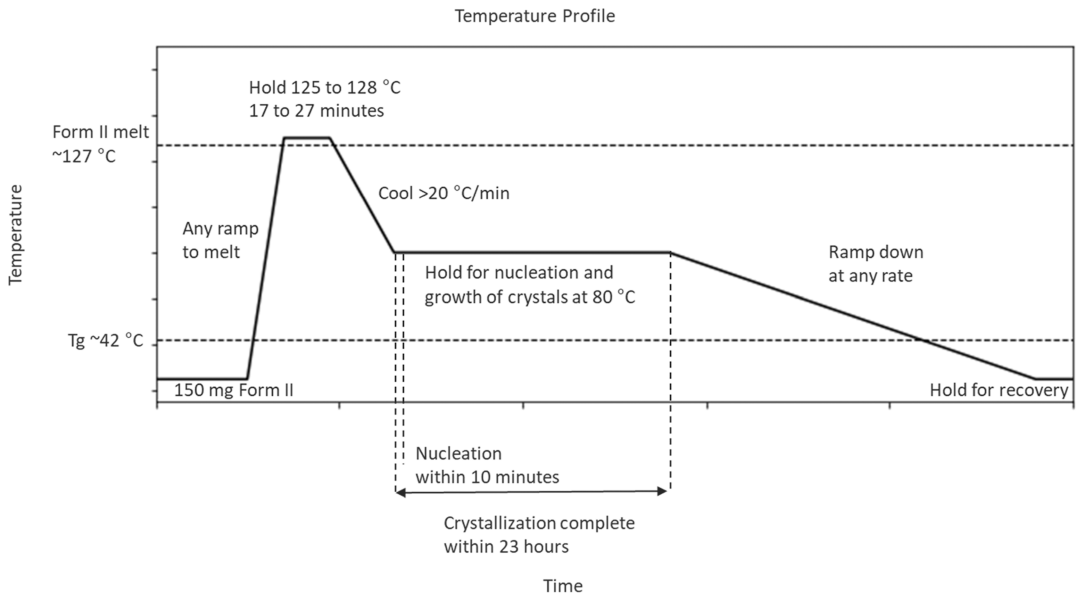

Figure 9. Temperature profile used to provide Form III ritonavir from a supercooled melt within 23 h.

the interplay of competing temperature-dependent thermophysical phenomena, there exists a local maximum corresponding to the highest crystallization rate achievable in a melt crystallization.[28,29] Cooling below the melting point not only increases saturation but also increases viscosity and reduces the available thermal energy that allows molecules to translate and rearrange in the melt. As a result, while undercooling to a greater degree increases the nucleation rate, eventually the increased viscosity and limited molecular mobility begin to suppress the nucleation rate. This work further reinforces the view of melt crystallization, by providing data showing that a maximum nucleation rate can be found, beyond which further cooling reduces the nucleation rate. By balancing the degree of undercooling with the temperature-dependent molecular mobility terms, the nucleation rate can be optimized.[28,29]

Figure 8 compares the crystal concentration after 5 and 8 h within the same supercooled melt when held at the ideal temperature, providing a visual representation of the relative crystallization rate achieved. Additional HSOM microcrystallization experiments also determined that (1) first nucleating Form III at a cooler temperature before incubating at a slightly higher temperature did not increase the overall rate of crystallization, while (2) the quench rate from the melt to the incubation temperature does influence the nucleation rate.

By applying a general rule of thumb, guidelines based on previously studied systems and the measured glass transition temperature of amorphous ritonavir, Yao et al. assumed that the maximum nucleation rate from the melt can only be achieved within a narrow temperature range of 60−70 °C.[25] As such, Yao et al. first nucleated Form III at 60 °C for 2 days and then continued its growth at 90 °C for an additional 2 days.[25] However, based on the empirical methodology our team developed, it was determined that these two temperatures are suboptimal for both nucleation and continued growth of Form III ritonavir from the supercooled melt. Rather, 80 °C was identified as both the ideal nucleation and ideal incubation temperature. Using the optimized conditions illustrated in Figure 9, our team was able to nucleate Form III ritonavir from the melt within a few hours at a microscale and was able to nucleate and completely crystallize Form III within 23 h at a macroscale.

CONCLUSIONS

While Form III appears to have been discovered as early as 2014, the recent detailed characterization, analysis, and reproduction of Form III ritonavir add to the allure of a notorious polymorph. Although it was previously claimed that Form III can only be nucleated between 60 and 70 ° C and crystallization takes 4 days to complete, this work demonstrates that performing the crystal growth at 80 °C reduces the total time to complete crystallization from the melt to less than 23 h.[25] Lastly, the presented work supports the conclusions of the Yao et al. publication that melt experiments are important for a comprehensive polymorph screening of ritonavir.[25]

ASSOCIATED CONTENT

Supporting Information

The Supporting Information is available free of charge at https://pubs.acs.org/doi/10.1021/acs.cgd.2c01017.

Experimental methods, additional characterization; hot-stage microscopy, dynamic vapor sorption, thermogravimetric analysis, and Raman spectra across a more limited range (PDF)

AUTHOR INFORMATION

Corresponding Author

Adrian Radocea − *Varda Space Industries, El Segundo, California 90245, United States;* orcid.org/0000-0002-4496-2573; Email: adrian@varda.com

Authors

Stephan D. Parent − *Improved Pharma LLC, West Lafayette, Indiana 47906, United States*

Pamela A. Smith − *Improved Pharma LLC, West Lafayette, Indiana 47906, United States*

Dale K. Purcell − *Improved Pharma LLC, West Lafayette, Indiana 47906, United States*

Daniel T. Smith − *Improved Pharma LLC, West Lafayette, Indiana 47906, United States*

https://doi.org/10.1021/acs.cgd.2c01017
Cryst. Growth Des. 2023, 23, 320−325

Susan J. Bogdanowich-Knipp − *Improved Pharma LLC, West Lafayette, Indiana 47906, United States*
Ami S. Bhavsar − *Varda Space Industries, El Segundo, California 90245, United States*
Larry R. Chan − *Varda Space Industries, El Segundo, California 90245, United States*
Jordan M. Croom − *Varda Space Industries, El Segundo, California 90245, United States*
Haley C. Bauser − *Varda Space Industries, El Segundo, California 90245, United States;* orcid.org/0000-0002-9677-3301
Andrew McCalip − *Varda Space Industries, El Segundo, California 90245, United States*
Stephen R. Byrn − *Improved Pharma LLC, West Lafayette, Indiana 47906, United States*

Complete contact information is available at: https://pubs.acs.org/10.1021/acs.cgd.2c01017

Author Contributions

The manuscript was written through contributions of all authors. All authors have given approval to the final version of the manuscript.

Notes

The authors declare the following competing financial interest(s): Varda Space Industries participated in the experimental design, research, data interpretation and analysis, writing, reviewing, and approval of the publication. A.S. Bhavsar, L.R. Chan, J.M. Croom, H.C. Bauser, A. McCalip, and A. Radocea are employees of Varda Space Industries and may own Varda Space Industries stock.

REFERENCES

(1) Bauer, J.; Spanton, S.; Henry, R.; Quick, J.; Dziki, W.; Porter, W.; Morris, J. Ritonavir: An Extraordinary Example of Conformational Polymorphism. *Pharm. Res.* **2001**, *18*, 859−866.
(2) Bučar, D. K.; Lancaster, R. W.; Bernstein, J. Disappearing Polymorphs Revisited. *Angew. Chem. Int. Ed.* **2015**, *54*, 6972−6993.
(3) Chemburkar, S. R.; Bauer, J.; Deming, K.; Spiwek, H.; Patel, K.; Morris, J.; Henry, R.; Spanton, S.; Dziki, W.; Porter, W.; Quick, J.; Bauer, P.; Donaubauer, J.; Narayanan, B. A.; Soldani, M.; Riley, D.; McFarland, K. Dealing with the Impact of Ritonavir Polymorphs on the Late Stages of Bulk Drug Process Development. *Org. Process Res. Dev.* **2000**, *4*, 413−417.
(4) Morissette, S. L.; Soukasene, S.; Levinson, D.; Cima, M. J.; Almarsson, O. Elucidation of Crystal form Diversity of the HIV Protease Inhibitor Ritonavir by High-throughput Crystallization. *Proc. Natl. Acad. Sci. U. S. A.* **2003**, *100*, 2180−2184.
(5) Dunitz, J. D.; Bernstein, J. Disappearing Polymorphs. *Acc. Chem. Res.* **1995**, *28*, 193−200.
(6) Beldjoudi, Y.; Arauzo, A.; Capo, J.; Gavey, E. L.; Pilkington, M.; Mascimento, M. A.; Rawson, J. M. Structural, Magnetic, and Optical Studies of the Polymorphic 9′-Anthrecenyl Dithiadiazolyl Radical. *J. Am. Chem. Soc.* **2019**, *141*, 6875−6889.
(7) Henck, J.; Bernstein, J.; Ellern, A.; Boese, R. Disappearing and Reappearing Polymorphs. The Benzocain:Picric Acid System. *J. Am. Chem. Soc.* **2001**, *123*, 1834−1841.
(8) Bernstein, J.; Henck, J. Disappearing and Reappearing Polymorphs − An Anathema to Crystal Engineering? *Cryst. Eng.* **1998**, *1*, 119−128.
(9) Blagden, N.; Davey, R. J.; Rowe, R.; Roberts, R. Disappearing Polymorphs and the Role of Reaction By-Products: The Case of Sulphathiazole. *Int. J. Pharm.* **1998**, *172*, 169−177.
(10) Bernstein, J. *Polymorphism in Molecular Crystals*, 2nd Edition; Oxford University Press, 2020.
(11) Lee, E. H. A Practical Guide to Pharmaceutical Polymorph Screening & Selection. *Asian J. Pharma. Sci.* **2014**, *9*, 163−175.
(12) Thorson, M. R.; Goyal, S.; Gong, Y.; Zhang, G. G. Z.; Kenis, P. J. A. Microfluidic Approach for Polymorph Screening Through Antisolvent Crystallization. *Cryst. Eng. Commun.* **2012**, *14*, 2404−2412.
(13) Gu, C.; Li, H.; Gandhi, R. B.; Raghavan, K. Grouping Solvents by Statistical Analysis of Solvent Property Parameters: Implication to Polymorph Screening. *Int. J. Pharm.* **2004**, *283*, 117−125.
(14) Solanki, P. V.; Uppello, S. B.; Dhokrat, P. A.; Bembalkar, S. F.; Mathad, V. T. Investigation on Polymorphs of Apixaban, an Anticoagulant Drug: Study of Phase Transformations and Designing Efficient Process for their Preparation. *World J. Pharm. Sci.* **2015**, *3*, 663−677.
(15) Alleso, M.; van den Berg, F.; Cornett, C.; Jorgensen, F. S.; Halling-Sorensen, B.; Lopez de Diego, H.; Hovhaard, L.; Aaltonan, J.; Rantanen, J. Solvent Diversity in Polymorph Screening. *J. Pharm. Sci.* **2008**, *97*, 2145−2159.
(16) Aaltonen, J.; Rantanen, J.; Siiria, S.; Karjalainen, M.; Jorgensen, A.; Laitinen, N.; Savolainen, M.; Seitavuopio, P.; Louhi-Kultanen, M.; Yliruusi, J. Polymorph Screening Using Near-Infrared Spectroscopy. *Anal. Chem.* **2003**, *75*, 5267−5273.
(17) Neumann, M. A.; van de Streek, J.; Fabbiani, F. P. A.; Hidber, P.; Grassmann, O. Combined Crystal Structure Prediction and High-Pressure Crystallization in Rational Pharmaceutical Polymorph Screening. *Nat. Commun.* **2015**, *6*, 7793.
(18) Jia, S.; Gao, Z.; Tian, N.; Li, Z.; Gong, J.; Wang, J.; Rohani, S. Review of Melt Crystallization in the Pharmaceutical Field, Towards Crystal Engineering and Continuous Process Development. *Chem. Eng. Res. Des.* **2021**, *166*, 268−280.
(19) Tian, B.; Gao, W.; Tao, X.; Tang, X.; Talyor, L. S. Impact of Polymers on the Melt Crystal Growth Rate of Indomethacin Polymorphs. *Cryst. Growth Des.* **2017**, *17*, 6467.
(20) Gunn, E.; Guzei, I. A.; Cai, T.; Yu, L. Polymorphism of Nifedipine: Crystal Structure and Reversible Transition of the Metastable β Polymorph. *Cryst. Growth Des.* **2012**, *12*, 2037−2043.
(21) Purohit, H. S.; Talyor, L. S. Phase Behavior of Ritonavir Amorphous Solid Dispersions During Hydration and Dissolution. *Pharm. Res.* **2017**, *34*, 2842−2861.
(22) Law, D.; Schmitt, E. A.; Marsh, K. C.; Everitt, E. A.; Want, W.; Fort, J. J.; Krill, S. L.; Qiu, Y. Ritonavir-PEG 8000 Amorphous Solid Dispersions: In Vitro and In Vivo Evaluations. *J. Pharm. Sci.* **2004**, *93*, 563−570.
(23) Trasi, N. A.; Bhujbal, S.; Zhou, Q. T.; Talyor, L. S. Amorphous Solid Dispersion Formation via Solvent Granulation − A Case Study with Ritonavir and Lopinavir. *Int. J. Pharm.* **2019**, *1*, No. 100035.
(24) Kawakami, K.; Harada, T.; Miura, K.; Yoshihashi, Y.; Yonemochi, E.; Terada, K.; Moriyama, H. Relationship Between Crystallization Tendencies During Cooling from Melt and Isothermal Storage: Toward a General Understanding of Physical Stability of Pharmaceutical Glasses. *Mol. Pharmaceutics* **2014**, *11*, 1835−1843.
(25) Yao, X.; Henry, R. F.; Zhang, G. G. Z. Ritonavir Form III: A New Polymorph After 24 Years. *Chem Rxiv* **2022**, DOI: 10.26434/chemrxiv-2022-35fwp.
(26) Coelho, A. A. Indexing of Powder Diffraction Patterns by Iterative use of Singular Value Decomposition. *J. Appl. Crystallogr.* **2003**, *36*, 86−95.
(27) Pawley, G. S. Unit Cell Refinement from Powder Diffraction Scans. *J. Appl. Crystallogr.* **1981**, *14*, 357−361.
(28) Davey, R.; Garside, J. *From Molecules to Crystallizers: An Introduction to Crystallization*; Oxford Science Publications, 2006
(29) Barham, P. J. Nucleation behavior of poly-3-hydroxybutyrate. *J. Mater. Sci.* **1992**, *19*, 3826−3834.